Mol Neurobiol
DOI 10.1007/s12035-016-9885-3

Phosphoinositides: Two-Path Signaling in Neuronal Response to Oligomeric Amyloid β Peptide

Romina María Uranga[1,2,3] · **Natalia Paola Alza**[1,2,3] · **Melisa Ailén Conde**[1,2,3] · **Silvia Susana Antollini**[1,2,3] · **Gabriela Alejandra Salvador**[1,2,3]

Received: 22 December 2015 / Accepted: 28 March 2016

Abstract We have previously demonstrated that oligomeric amyloid β peptide (oAβ) together with iron overload generates synaptic injury and activation of several signaling cascades. In this work, we characterized hippocampal neuronal response to oAβ. HT22 neurons exposed to 500 nM oAβ showed neither increased lipid peroxidation nor altered mitochondrial function. In addition, biophysical studies showed that oAβ did not perturb the lipid order of the membrane. Interestingly, although no neuronal damage could be demonstrated, oAβ was found to trigger bifurcated phosphoinositide-dependent signaling in the neuron, on one hand, the phosphorylation of insulin receptor, the phosphatidylinositol 3-kinase (PI3K)-dependent activation of Akt, its translocation to the nucleus and the concomitant phosphorylation, inactivation, and nuclear exclusion of the transcription factor Forkhead Box O3a (FoxO3a), and on the other, phosphoinositide-phospholipase C (PI-PLC)-dependent extracellular signal-regulated kinase 1/2 (ERK1/2) activation. Pharmacological manipulation of the signaling cascades was used in order to better characterize the role of oAβ-activated signals, and mitochondrial function was determined as a measure of neuronal viability. The inhibition of PI3K, PI-PLC, and general phosphoinositide metabolism impaired neuronal mitochondrial function. Furthermore, increased oAβ-induced cell death was observed in the presence of phosphoinositide metabolism inhibition. Our results allow us to conclude that oAβ triggers the activation of phosphoinositide-dependent signaling, which results in the subsequent activation of neuroprotective mechanisms that could be involved in the determination of neuronal fate.

Keywords Amyloid β peptide · Phosphoinositides · PI3K · FoxO · PI-PLC · ERK1/2

Abbreviations

AD	Alzheimer's disease
ANOVA	Analysis of variance
APP	Amyloid beta precursor protein
Aβ	Amyloid β peptide
BSA	Bovine serum albumin
DAG	Diacylglycerol
DCDCDHF	2′,7′-Dichlorofluorescein diacetate
DMEM	Dulbecco's modified Eagle's medium
DMSO	Dimethyl sulfoxide
DPH	1,6-diphenyl-1,3,5-hexatrien
DTT	Dithiothreitol
EDTA	Ethylenediaminetetraacetic acid
EM	Electron microscopy
ERK1/2	Extracellular signal-regulated kinases 1/2
FBS	Fetal bovine serum
FoxO3a	Forkhead Box O3a
GP	Generalized polarization
hNRP	Human NAP-related protein
HRP	Horseradish peroxidase

Natalia Paola Alza and Melisa Ailén Conde contributed equally to this work.

Electronic supplementary material The online version of this article (doi:10.1007/s12035-016-9885-3) contains supplementary material, which is available to authorized users.

✉ Gabriela Alejandra Salvador
salvador@criba.edu.ar

[1] Instituto de Investigaciones Bioquímicas de Bahía Blanca, La Carrindanga Km 7, 8000 Bahía Blanca, Buenos Aires, Argentina

[2] Universidad Nacional del Sur, Bahía Blanca, Argentina

[3] Consejo Nacional de Investigaciones Científicas y Técnicas, Bahía Blanca, Argentina

Published online: 14 April 2016

IR	Insulin receptor
LDH	Lactate dehydrogenase
LilrB2	Leukocyte immunoglobulin-like receptor B2
MAPK	Mitogen-activated protein kinase
MTT	3-(4,5-dimethylthiazol-2-yl)-2,5-diphenyl-tetrazolium bromide
oAβ	Oligomeric amyloid β peptide
PBS	Phosphate-buffered saline
PI	Phosphoinositide
PI3K	Phosphatidylinositol 3-kinase
PIP_2	Phosphatidylinositol bis-phosphate
PI-PLC	Phosphoinositide-phospholipase C
PrP^C	Cellular prion protein
TBA	Thiobarbituric acid
TBARS	Thiobarbituric acid-reactive substance
TCA	Trichloroacetic acid
TMA-DPH	1-(4-trimethylammoniumphenyl)-6-phenyl-1,3,5-hexatriene

Introduction

Memory impairment in Alzheimer's disease (AD) is associated with neuronal degeneration and, in the early stages, with synaptic damage and loss. In vivo experiments using transgenic animals demonstrate that amyloid β peptide (Aβ) is the main factor responsible for neuronal deterioration and death. Oligomeric Aβ (oAβ) in particular has been associated with the down-regulation of synaptic plasticity and density [1].

Despite the considerable effort invested in understanding the molecular mechanisms triggered by oAβ, there are still many unanswered questions. Exogenously added Aβ has been associated with diverse and non-homogeneous neuronal effects including increased synaptic activity, synaptic depression and toxicity, and also neuronal excitation [2–6]. These dissimilar effects have been attributed to the physical state of Aβ aggregation and the time of incubation.

One of the most intriguing effects of Aβ oligomers is their capacity to bind to several plasma membrane receptors [7]. Aβ oligomers act as partial agonists of β2 adrenergic receptor and activate specific downstream signaling through the generation of receptor conformational changes [8]. In PC12 cells, translocation to the cell membrane surface and activation of α7 acetylcholine receptor have been associated with cellular response to exogenous Aβ [9]. In this connection, it has been demonstrated that the activation of α7 acetylcholine receptor reverts the synaptic impairment triggered by Aβ oligomers [10]. Amyloid beta precursor protein (APP) has also been demonstrated to act as a receptor of Aβ-species which promotes toxicity in hippocampal neurons through the activation of intracellular pathways that involve G_o protein [11]. The modulation of the melatoninergic system and the inhibition of melatonin synthesis in the pineal gland have been also attributed to Aβ [12]. The receptor-gating properties of Aβ have been associated with increased activity, neuronal hyperactivity, and finally neuronal death [13]. These findings open a new window in the search for therapeutic strategies and engineered drugs that target membrane receptors able to bind to and be activated by oAβ [7, 13, 14].

In previous work, using in vitro experiments, we reported that oAβ alone or complexed with transition metals (Fe and Cu) is able to induce synaptic injury and to trigger the activation of the phosphoinositide 3-kinase (PI3K)/Akt pathway and also the extracellular signal-regulated kinases 1 and 2 (ERK1/2). Synaptic PI3K activation was observed in the presence of increased membrane permeability and mitochondrial dysfunction [15]. PI3K was also activated by oxidative injury elicited by iron overload in synaptic endings and hippocampal neurons [15, 16]. The activation of PI3K under oxidative stress conditions has a neuroprotective role through the regulation of pleiotropic targets by inhibiting Forkhead Box O3a (FoxO3a) transcriptional activity on the one hand and regulating phase II antioxidant defenses on the other. In line with this, sustained PI3K activation has been associated with toxic forms of Aβ and altered tau phosphorylation. The reduction in PI3K activation by blocking insulin receptor and insulin-like growth factor renders less toxic protein conformations and also improves cognitive function [17].

Based on this mounting evidence, our aim in the present study was to characterize phosphoinositide (PI)-dependent signaling pathways in the neuronal response to oAβ exposure. For this purpose, we worked with HT22 hippocampal neurons exposed to nanomolar concentrations of oAβ for 24 h. As a first step, cellular status was evaluated through biochemical, cell biology, and biophysical studies, after which we determined the state of the above-mentioned pathways and their role in the neuronal response to oAβ.

Materials and Methods

Materials

Rat amyloid β peptide 1–40 ($Aβ_{1–40}$) was purchased from Tocris (Ellisville, MO; catalog no. 2424). 2′,7′-Dichlorofluorescein diacetate (DCDCDHF; catalog no. D399), 6-dodecanoyl-2-dimethylaminonaphthalene (Laurdan; catalog no. D-250), 1-(4-trimethylammoniumphenyl)-6-phenyl-1,3,5-hexatriene (TMA-DPH; catalog no. T-204), and SYTOX green dye (catalog no. S-7020) were obtained from Molecular Probes (Eugene, OR, USA). Thiobarbituric acid (TBA; catalog no. T5500), dimethyl sulfoxide (catalog no. D2650), 2-(4-morpholinyl)-8-phenyl-1(4H)-benzopyran-4-one hydrochloride (LY294002; catalog no. L9908), 3-(4,5-dimethylthiazol-2-yl)-2,5-diphenyltetrazolium bromide (MTT; catalog no. M2128), 1-[6((17b-3-methoxyestra-1,3,5(10)-

trien-17-yl)-amino)hexyl]-1H-pyrrole-2,5-dione (U73122; catalog no. U6756), 2′-(4-ethoxyphenyl)-5-(4-methyl-1-piperazinyl)-2,5′-bi-1H-benzimidazole trihydrochloride (Hoechst; catalog no. 14533), neomycin (catalog no. N1876), 1,6-diphenyl-1,3,5-hexatriene (DPH; catalog no. D4380), caspase 3 substrate (Ac-DEVD-pNA; catalog no. A2559), and Triton™ X-100 (catalog no. T9284) were purchased from Sigma Aldrich Co. (St. Louis, MO, USA). Bovine serum albumin (BSA) was purchased from Santa Cruz Biotechnology. Edelfosine (ET-18-OCH_3; catalog no. 341207) was purchased from Calbiochem. PD98059 (catalog no. 10006726) was purchased from Cayman Chemical. The kit (LDH-P UV AA) for measuring lactate dehydrogenase (LDH) activity was generously supplied by the Wiener Laboratory (Rosario, Santa Fe, Argentina; catalog no. 1521303). All other chemicals used in the present study were of the highest purity available.

Antibodies mouse monoclonal anti-β-actin (catalog no. 47778), human NAP-related protein (hNRP; catalog no. 32301), polyclonal horse radish peroxidase (HRP)-conjugated goat anti-mouse IgG (catalog no. 2005), and polyclonal HRP-conjugated goat anti-rabbit IgG (catalog no. 2004) were purchased from Santa Cruz Biotechnology; rabbit polyclonal anti-phosphoSer473-Akt (catalog no. 9271), rabbit polyclonal anti-Akt (catalog no. 9272), rabbit polyclonal anti-FoxO3a (catalog no. 2497), rabbit polyclonal phosphoSer253-FoxO3a (catalog no. 9466), rabbit polyclonal anti-phosphoThr202/Tyr204-ERK1/2 (catalog no. 9101), rabbit polyclonal anti-phosphoThr638/641-PKCα/βII (catalog no. 9375), rabbit monoclonal anti-insulin receptor β (catalog no. 3025), and monoclonal rabbit anti-phosphoTyr1361-insulin receptor β (catalog no. 3023) were purchased from Cell Signaling Technology; and polyclonal Alexa Fluor® 488-conjugated goat anti-rabbit (catalog no. A-11034) and polyclonal Alexa Fluor® 488-conjugated goat anti-mouse (catalog no. A-11029) were purchased from Life Technologies (Thermo Fisher Scientific). OC and A11 antibodies were a kind gift from Dr. Charles Glabe (Department of Molecular Biology and Biochemistry, University of California, Irvine, USA).

Cell Culture

HT22 murine hippocampal neuronal cells were used for the experiments. Cells were cultured in Dulbecco's modified Eagle's medium (DMEM; Gibco, Thermo Fisher Scientific, Argentina) supplemented with 10 % fetal bovine serum (FBS; Natocor, Argentina), 100 U/ml penicillin, 100 μg/ml streptomycin, and 0.25 μg/ml amphotericin B (Gibco, Thermo Fisher Scientific, Argentina) at 37 °C in humidified atmosphere containing 5 % CO_2. For all the experiments, cells were grown to 80–90 % confluence. Before the treatments, the medium was replaced by serum-free medium.

Experimental Treatments

Depending on the sensitivity of the different methodologies, cells were plated in either 35 × 10-mm cell culture dishes or 24-well cell culture plates and grown to 80–90 % confluence. oAβ treatments were carried out in serum-free medium for 24 h.

Pharmacological Manipulation of Signaling Cascades

Treatments with LY294002, U73122, U0126, PD98059, edelfosine, and neomycin were performed as follows: medium was removed and replaced by serum-free media; inhibitors were then added to the desired final concentration (controls received vehicle alone); and, after 30 min, oAβ was added and cells were incubated under these conditions for 24 h. Final concentrations of the inhibitors in the medium were 10 μM U73122, 10 μM LY294002, 10 μM U0126, 10 μM PD98059, 2.5 μM edelfosine, and 200 μM neomycin.

$A\beta_{1–40}$ Peptide Preparation

$A\beta_{1–40}$ was resuspended in dimethyl sulfoxide (DMSO) at a concentration of 10 mg/ml (peptide stock solution) and immediately stored in aliquots at -80 °C. Aβ oligomers were prepared immediately prior to use (working solution) according to previously published methods [15, 18, 19]. Briefly, aliquots of peptide stock (10 μl) were added to 280 μl of phosphate-buffered saline (PBS; pH 7.4) and stirred continuously (300 rpm, at 37 °C) for 120 min and stored at 4 °C until use.

Electron Microscopy

Electron microscopy (EM) studies were carried out according to previously published methods with slight modifications [15, 18]. Briefly, 500 nM oAβ was incubated in PBS at 37 °C for 24 h. After incubation, 10 μl of media containing the peptide was placed on a carbon-coated grid and incubated for 60 s. Ten microliters of 0.5 % glutaraldehyde was added to the grid followed by incubation for an additional 60 s. The grid was then washed with drops of water and dried. Finally, the grid was stained for 2 min with 2 % uranyl acetate and then air dried. The grid was subsequently examined under a Jeol 100 Cx II electron microscope.

Dot Blot

One microliter (lane 1), 4 μl (lane 2), or 10 μl of oAβ preparation was loaded onto nitrocellulose membrane and probed with the A11 and OC antibodies. These antibodies do not recognize specific amino acid sequences, but conformational epitopes: A11 antibodies are specific for prefibrillar oligomers and OC antibodies recognize fibril-like oligomers [20].

Cell Viability Assay

Cell viability was assessed using the MTT reduction assay. MTT is a water-soluble tetrazolium salt that is reduced by metabolically viable cells to a colored, water-insoluble formazan salt [16]. After treatments, MTT (5 mg/ml, diluted in PBS) was added to the cell culture medium at a final concentration of 0.5 mg/ml. After incubating the plates for 2 h at 37 °C in a 5 % CO_2 atmosphere, the assay was stopped and the MTT-containing medium was replaced by solubilization buffer (20 % SDS, pH 4.7). The extent of MTT reduction was measured spectrophotometrically at 570 nm.

Determination of Lipid Peroxidation

Lipid peroxidation was determined by the thiobarbituric acid reactive substance (TBARS) assay, which involves derivatization of malondialdehyde with TBA to produce a pink product that is quantified in a UV–Vis spectrophotometer [16]. Briefly, after treatments, cells were scraped off into 200 μl of ice-cold water and mixed with 0.5 ml of 30 % trichloroacetic acid (TCA). Fifty microliter of 5 N HCl and 0.5 ml of 0.75 % thiobarbituric acid were then added. Tubes were capped, the mixtures were heated at 100 °C for 15 min in a boiling water bath, and the samples were centrifuged at 1000×*g* for 10 min. TBARSs were measured spectrophotometrically in the supernatant at 535 nm.

Determination of Cell Oxidant Levels

Cell oxidant levels were evaluated using the probe DCDCDHF [16]. This probe can cross the membrane and after oxidation, is converted into a fluorescent compound. Following the corresponding treatments, the media were discarded and complex medium containing 10 μM DCDCDHF was added. After 30 min of incubation at 37 °C, the medium was removed and cells were rinsed three times with PBS and then lysed in a buffer containing PBS and 1 % Nonidet P-40 (NP-40). Fluorescence in the lysates (λ_{ex} = 495, λ_{em} = 530 nm) was measured in a SLM model 4800 spectrofluorimeter (SLM Instruments, Urbana, IL).

Measurement of LDH Release

LDH leakage was determined as previously described [21, 22] with slight modifications. After treatments, the incubation medium was centrifuged at 1000×*g* for 10 min at 4 °C. The resulting supernatant was used to determine LDH activity, which was measured spectrophotometrically using an LDH-P UV AA Kit, following the manufacturer's instructions. Briefly, the conversion rate of reduced nicotinamide adenine dinucleotide to oxidized nicotinamide adenine dinucleotide was followed at 340 nm.

Caspase 3 Activity

Caspase 3 activity was assessed according to Hanzel and Verstraeten [23] with minor modifications. Briefly, after treatments, cells from two 35-mm-diameter cell culture dishes were collected by scraping in PBS and centrifuged for 10 min at 1000×*g* at 4 °C. Pellets were suspended in a 50 mM HEPES buffer (pH 7.4) containing 0.1 % NP-40, 1 mM dithiothreitol (DTT), 0.1 mM ethylenediaminetetraacetic acid (EDTA), and 150 mM NaCl and incubated on ice for 5 min. Samples were centrifuged at 12,000×*g* for 10 min at 4 °C. Protein content was measured in supernatants [24]. Samples containing 150-200 μg protein were incubated in the presence of 10 % (*v*/*v*) glycerol and 0.2 mM of caspase 3 substrate (Ac-DEVD-pNA) overnight at 37 °C. The formation of p-nitroanilide was registered at 405 nm.

Biophysical Studies

Fluorescence Measurements

After treatments, cells were washed with PBS and collected, dissociated, and kept in a buffer containing PBS and 5 mM EDTA (pH 7.4) at 37 °C during the whole experiment. The optical density of the cell suspension was kept below 0.1 to minimize light scattering. All fluorimetric measurements were performed in an SLM model 4800 spectrofluorimeter (SLM Instruments, Urbana, IL) using a vertically polarized light beam from Hannovia 200-W mercury/xenon arc obtained with a Glan-Thompson polarizer (4-nm excitation and emission slits) and 1-ml quartz cuvettes. The temperature was set at 37 °C with a thermostated circulating water bath (Haake, Darmstadt, Germany).

Generalized Polarization Determination

Laurdan was added to the cell suspension (80–100 μg protein/ml) of an ethanol solution to give a final probe concentration of 0.3 μM. The amount of organic solvent was kept below 0.1 %. The samples were incubated at 37 °C for 1 h in the dark to allow equilibration, and then, the emission spectra were collected. Generalized polarization (GP) values were obtained from emission spectra using an excitation wavelength of 360 nm and calculated as follows:

$$GP = (I_{434} - I_{490})/(I_{434} + I_{490})$$

where I_{434} and I_{490} are the emission intensities at the characteristic wavelength of the gel and liquid-crystalline phases, respectively [25, 26].

Anisotropy Measurements

The fluorescence probe DPH or TMA-DPH was added to the cell suspension (80–100 μg protein/ml) to give a final concentration of 0.3 μM. The samples were incubated at 37 °C for 30 min in the dark to allow equilibration before anisotropy (r) measurements. The excitation and emission wavelengths were 364 and 426 nm, respectively. Fluorescence anisotropy measurements were carried out in the T format with Schott KV418 filters in the emission channels and corrected for optical inaccuracies and background signals. The anisotropy value, r, was obtained according to the following equation:

$$r = \left(\left(I_v/I_h\right)_v - \left(I_v/I_h\right)_h\right)\Big/\left(\left(I_v/I_h\right)_v + I_v/I_h\right)_h\Big)$$

where $(I_v/I_h)_v$ and $(I_v/I_h)_h$ are the ratios of the emitted vertical or horizontally polarized light to the exciting, vertical or horizontally polarized light, respectively. The r value can range between −0.2 and 0.4, higher values denoting higher structural lipid order [27].

Western Blot Analysis

For the preparation of total cell extracts, cells (10×10^6 cells) were rinsed with PBS, scraped, and centrifuged. The pellet was rinsed with PBS and resuspended in 200 μl of a buffer containing 50 mM Tris, pH 7.5, 150 mM NaCl, 0.1 % Triton X-100, 1 % NP-40, 2 mM EDTA, 2 mM EGTA, 50 mM NaF, 2 mM β-glycerophosphate, 1 mM Na_3VO_4, 10 μg/ml leupeptin, 5 μg/ml aprotinin, 1 μg/ml pepstatin, 0.5 mM PMSF, and 0.5 mM DTT. Samples were exposed to one cycle of freezing and thawing, incubated at 4 °C for 30 min, and centrifuged at 15,000×g for 30 min. The supernatant was decanted and the protein concentration was measured [24]. Aliquots of the lysate containing 25–50 μg of protein were separated by reducing 7–12.5 % polyacrylamide gel electrophoresis and electroblotted to polyvinylidene difluoride membranes (Millipore). Molecular weight standards (Spectra™ Multicolor Broad Range Protein Ladder, Thermo Scientific) were run simultaneously. Membranes were blocked with 5 % non-fat dry milk or 2–5 % BSA in TBS-T buffer (20 mM Tris–HCl (pH 7.4), 100 mM NaCl, and 0.1 % (w/v) Tween 20) for 2 h at room temperature and then incubated with primary antibodies overnight at 4 °C, washed three times with TBS-T buffer, and then exposed to the appropriate HRP-conjugated secondary antibody for 1 h at room temperature. Membranes were again washed three times with TBS-T buffer, and immunoreactive bands were detected by enhanced chemiluminescence (ECL; GE Healthcare Bio-Sciences, Buenos Aires, Argentina) using standard X-ray film (Hyperfilm ECL; GE Healthcare Bio-Sciences). Immunoreactive bands were quantified using image analysis software (ImageJ, a freely available application in the public domain for image analysis and processing, developed, and maintained by Wayne Rasband at the Research Services Branch, National Institute of Mental Health).

Cytoplasmic and Nuclear Fractionation with Nonidet P-40 Detergent-Containing Buffer

Nuclear and cytosolic fractions were isolated as described previously [16, 28, 29]. After treatments, the medium was discarded and cells were rinsed with PBS and scraped. After centrifugation at 800×g for 10 min, the pellet (10×10^6 cells) was resuspended in 100 μl of buffer A (10 mM HEPES (pH 7.9), 1.5 mM $MgCl_2$, 10 mM KCl, 0.5 mM DTT, 0.1 % NP-40, 2 μg/μl leupeptin, 1 μg/μl aprotinin, and 1 μg/μl pepstatin), incubated for 10 min at 4 °C, and centrifuged for 2 min at 12,000×g. The supernatant (cytosolic fraction) was removed, and the nuclear pellet was resuspended in 40 μl of buffer B (10 mM HEPES (pH 7.9), 1.5 mM $MgCl_2$, 420 mM NaCl, 0.5 mM DTT, 0.2 mM EDTA, 25 % glycerol, 0.5 mM PMSF, 2 μg/ml leupeptin, 1 μg/ml aprotinin, and 1 μg/ml pepstatin). Samples were incubated for 20 min at 4 °C and centrifuged at 10,000×g for 15 min at 4 °C. Protein concentration was determined by the method of Bradford [24], and samples were stored at −20 °C until used for Western blot analyses.

Immunofluorescence Microscopy

HT22 cells were grown onto glass coverslips, and the growing medium was replaced by serum-free medium. After treatment with 500 nM oAβ for 24 h, the cells were fixed with 4 % paraformaldehyde for 15 min at room temperature, followed by three washes with PBS, three washes with 30 mM glycine/PBS (pH 7.4), and three additional washes with PBS. For the immunostaining, cells were permeabilized and the non-specific sites were blocked with 5 % BSA/0.3 % Triton X-100/PBS (pH 7.4) at room temperature for 1 h. Cells were incubated with the appropriate primary antibody (1:50 in 1 % BSA/0.3 % Triton X-100/PBS; 1 h at room temperature). After three washes with PBS, cells were incubated with the appropriate Alexa Fluor® 488-conjugated secondary antibody (1:200 in 1 % BSA/PBS; 1 h at room temperature) and Hoechst for nuclear staining. After washing with PBS at room temperature for 10 min, coverslips were mounted and slides were observed with a Nikon Eclipse E-600 microscope (Nikon, Melville, NY, USA), using a K2E Apogee CCD camera driven by CCDOPS software (Santa Barbara Instrument Group, Santa Barbara, CA, USA).

SYTOX Green Fluorescent Nucleic Acid Stain

SYTOX is a green nucleic acid stain that is impermeable to live cells, making it a useful indicator of dead cells within a population. It easily penetrates cells with compromised plasma membranes but will not cross the membranes of live cells. Cells were grown onto glass coverslips as for immunocytochemistry studies, following which they were treated with SYTOX green dye to a final concentration of 2 nM, and after a 10–20-min incubation, washed three times in PBS, and fixed with 4 % paraformalhehyde. Nuclei were counterstained with Hoechst. Finally, coverslips were mounted and slides were observed in a fluorescence microscope.

Statistical Analysis

Quantitative results were expressed as the mean ± standard error of measurement. Table 1 and Figs. 2a, e, f and 4a, b were analyzed by Student's *t* test. Figures 3a–c, 4c–e, 5a–c, 6a, b, and 7a were analyzed by one-way analysis of variance (ANOVA) to determine group differences, followed by Tukey's post hoc analysis to determine specific differences between conditions. Statistical significance for all analyses was accepted at $p < 0.05$, and * (or $^{\#}$), ** (or $^{\#\#}$), and *** (or $^{\#\#\#}$) represent $p < 0.05$, $p < 0.01$, and $p < 0.001$, respectively. Western blots, photomicrographs, and immunocytochemistry images are representative of at least three analyses performed on samples from at least three separate experiments.

Results

Aggregation of Aβ

oAβ was prepared following a method previously published by our group and others and stored at −80 °C [15, 18, 19]. The quality of oligomer working solution was examined both by EM (Fig. 1a) and dot blot analysis (Fig. 1b). EM photomicrographs show that Aβ preparations included spheroidal structures individually or in small groups (Fig. 1a). These ultrastructural forms were compatible with a heterogeneous array of oligomers discarding the presence of fibrils. Dot blot analysis of Aβ solutions using A11 and OC antibodies indicate that our Aβ preparations were positive for OC antibodies. This indicates that Aβ preparations were mainly composed of fibril-like oligomers also known as Aβ-type 2 oligomers (Fig. 1b). Dopaminergic neurons overexpressing α-synuclein were used to test A11 antibody reactivity (data not shown).

Table 1

Parameter	Control (arbitrary units)	Aβ (arbitrary units)
MTT reduction	0.632 ± 0.012	0.638 ± 0.020
TBARS	0.021 ± 0.003	0.025 ± 0.004
Cell oxidants	169.796 ± 17.003	160.716 ± 24.993
LDH leakage	0.062 ± 0.002	0.064 ± 0.002
Caspase 3 activity	0.181 ± 0.019	0.1659 ± 0.040
r (DPH)	0.222 ± 0.007	0.230 ± 0.001
r (TMA-DPH)	0.298 ± 0.001	0.293 ± 0.001
GP (Laurdan)	0.364 ± 0.015	0.372 ± 0.013

Effects of oAβ Exposure on Neuronal Integrity

We have previously characterized the effect of oAβ exposure on isolated synaptic endings [15]. In this report, we exposed mouse hippocampal neurons (HT22) to 500 nM oAβ for 24 h and different biochemical and biophysical approaches were used to determine neuronal status. The control conditions were also assessed, replacing oAβ with an equal volume of the vehicle. As seen in Fig. 1c, no morphological changes were detected in those neurons exposed to oAβ with respect to the control. In addition, markers of neuronal function and integrity such as MTT mitochondrial reduction, lipid peroxidation levels, and LDH leakage were unchanged in neurons exposed to oAβ when compared with control cultures (Table 1). In order to determine whether oAβ triggers membrane property perturbations, we studied the membrane lipid order of cells under different experimental conditions. To this end, DPH and TMA-DPH anisotropy and Laurdan GP were evaluated. DPH, an apolar molecule, inserts deep inside the hydrophobic core of the membrane, whereas TMA-DPH, which has a positively charged amino group, anchors near the surface of the external hemilayer [30]. The third probe, Laurdan, locates superficially in both hemilayers because of a rapid flip-flop between them. Thus, through parallel spectroscopic experiments using these three fluorescence probes, we could evaluate both the superficial and deep membrane order. As seen in Table 1, no alteration of the lipid order of the membrane was observed. Additionally, caspase 3 activity was determined as apoptotic marker and no changes were observed in neurons exposed to oAβ. Based on these results, we postulate that oAβ at the nanomolar range does not provoke any noticeable damage in hippocampal HT22 neurons.

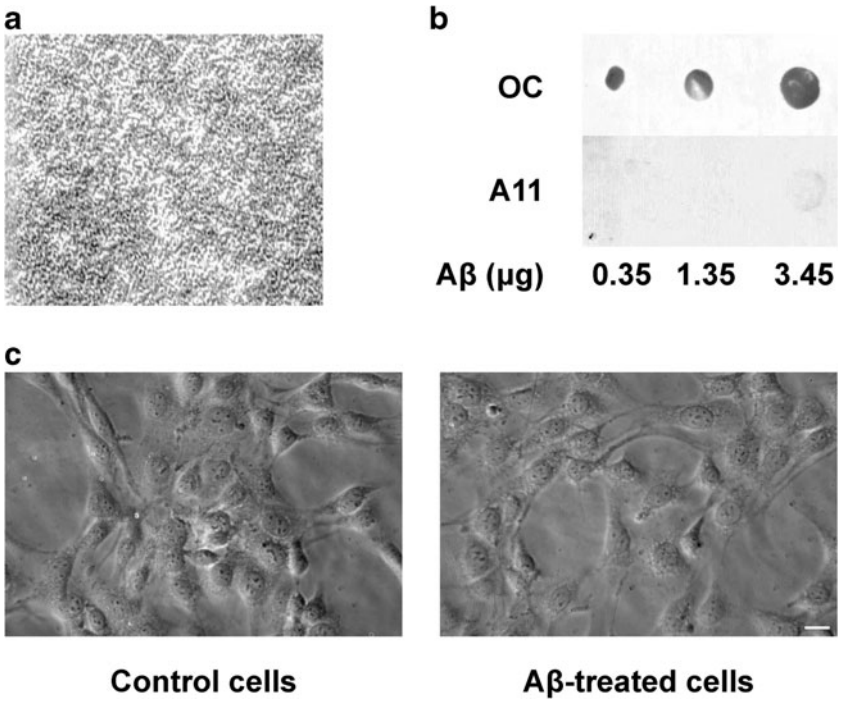

Fig. 1 Characterization of oAβ preparation. **a** High-power (×140,000) electron photomicrograph showing oAβ preparation. Aβ oligomers were prepared as described in "Materials and Methods" section. **b** *Dot* blot showing oligomeric forms of Aβ preparation. **c** Micrographs of HT22 cells treated with 500 nM oAβ or vehicle for 24 h. *Scale bar* 10 μm

Effect of oAβ Exposure on PI3K/Akt Signaling

We next investigated whether oAβ was able to trigger cellular signaling pathways known to be associated with the determination of cellular fate. First of all, we detected an increased tyrosine phosphorylation of the insulin receptor β subunit. The extent of oAβ-triggered phosphorylation of insulin receptor (200 % of the control) was coincident with that found in the phosphorylation of Akt, a well-known downstream target of PI3K (Fig. 2a).

Since we have previously demonstrated that the PI3K/Akt pathway undergoes not only activation but also subcellular redistribution under neuronal oxidative stress conditions, we sought to determine whether the activation of insulin receptor and the PI3K/Akt pathway were accompanied by differential cellular compartmentalization or redistribution of its components after oAβ treatment. Analyses of immunocytochemistry studies clearly show that oAβ did not affect insulin receptor subcellular distribution (Fig. 2b) but it did generate both PI3K and Akt translocation from the cytosol to the nucleus compared to the control condition (Fig. 2c, d, e). PI3K subcellular redistribution was also studied using Aβ which was not subjected to the process of oligomerization. Non-oligomerized Aβ showed no effect on PI3K subcellular distribution (Supplementary Fig. 1). Moreover, nuclear increases of PI3K and Akt were also confirmed by Western blot studies carried out in the nuclear fraction of both control and oAβ-treated cells (Fig. 2f).

Consequences of oAβ Exposure on FoxO3a Transcription Factor

We next investigated whether oAβ-triggered PI3K and Akt nuclear translocation was dependent on PI3K activation. For this purpose, we used LY294002, a known PI3K inhibitor, in our experiments. Western blots shown in Fig. 3a demonstrate that both PI3K and Akt subcellular redistributions were strictly dependent on PI3K activation.

We have previously demonstrated that PI3K/Akt nuclear localization as a neuronal response to oxidative stress determines the nuclear exclusion of the FoxO3a transcription factor [16]. Based on these data and on the fact that PI3K/Akt was shown to translocate to the nucleus in response to oAβ, we next investigated whether oAβ exerted any PI3K-dependent effects on FoxO3a. Immunocytochemistry experiments show that in the absence of oAβ, FoxO3a was mainly located in the nucleus, but that upon Aβ treatment, although still present in the nucleus, it was more abundant in the cytosol (Fig. 3b). This redistribution of FoxO3a was found to be dependent on PI3K activity, since the presence of LY294002 abolished the oAβ-induced movement of the transcription factor out of the nucleus (Fig. 3b).

Since it is well known that FoxO3a phosphorylation is a prerequisite for its exclusion from the nucleus, we assessed the phosphorylation state of the transcription factor by Western blot studies. As shown in Fig. 3c, FoxO3a phosphorylation increased upon oAβ treatment in a PI3K-dependent manner.

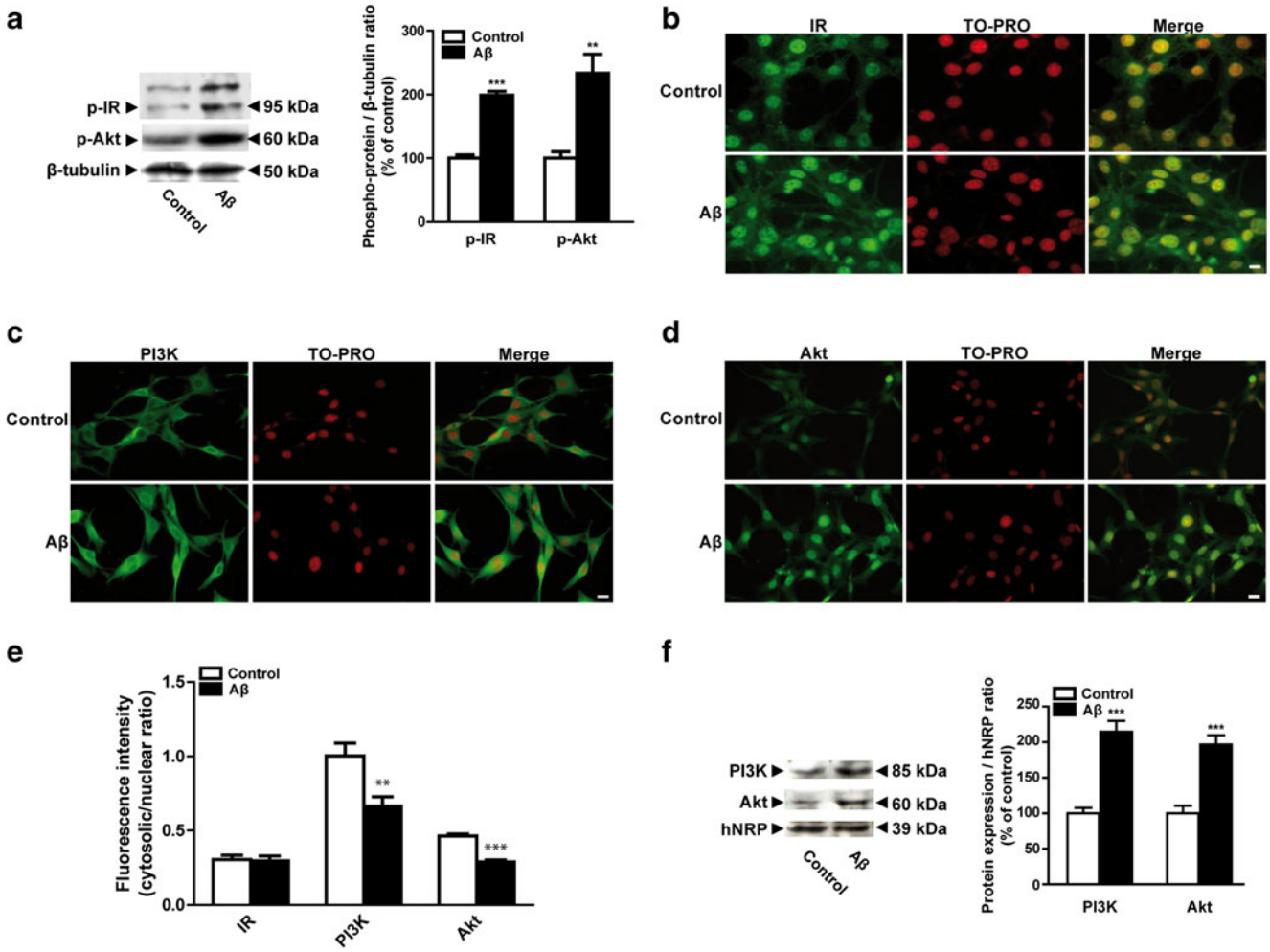

Fig. 2 Effect of oAβ exposure on insulin receptor (IR) and PI3K/Akt signaling. **a** Lysates from HT22 cells exposed to oAβ or its vehicle were studied by Western blot assays. IR and Akt phosphorylation was assessed. Each blot is representative of at least three different experiments. Bands of proteins were quantified using scanning densitometry; the data in the *graph on the right* represent the ratio between the phosphorylated protein and β-tubulin, expressed as a percentage of the corresponding control condition (mean ± SE of three different experiments). $^{**}p < 0.01$, $^{***}p < 0.001$ for each condition with respect to the control; Student's *t* test. **b**–**d** Immunocytochemistry studies were performed using anti-IR (**b**), anti-PI3K (**c**), and anti-Akt (**d**) antibodies in neurons treated with Aβ or its vehicle. TO-PRO was used as nuclear marker. The pictures shown are representative of at least three different experiments. *Scale bars* 10 μm. **e** Fluorescence intensity quantification of experimental conditions shown in **b**, **c**, and **d**. Fluorescence of approximately 100–150 cells was quantified for each condition in each experiment. $^{**}p < 0.01$, $^{***}p < 0.001$ for each condition with respect to the control; Student's *t* test. **f** Nuclear fractions of HT22 cells exposed to oAβ or its vehicle were analyzed by Western blot using antibodies against PI3K and Akt. hNRP was used as nuclear marker. The blots shown are representative of at least three different experiments. Bands of proteins were quantified using scanning densitometry; the data in the *graph on the right* represent the ratio between protein expression and hNRP, expressed as a percentage of the corresponding control condition (mean ± SE of three different experiments). $^{***}p < 0.001$ for each condition with respect to the control; Student's *t* test

Effects of oAβ Treatment on ERK1/2 Signaling

Like PI3K/Akt, ERK1/2 kinases play crucial roles in the determination of neuronal fate, and for this reason, we assessed whether oAβ also triggers this signaling cascade. Western blot studies show that neurons exposed to oAβ also displayed increased levels of ERK1/2 phosphorylation (200 % of the control; Fig. 4a).

We next investigated whether ERK1/2 activation was accompanied by cellular redistribution after oAβ treatment. Analysis of immunocytochemistry studies clearly shows that oAβ triggered ERK1/2 translocation from the cytosol to the nucleus compared to the control condition (Fig. 4b). Moreover, analysis of Western blot studies carried out in the cytosolic and nuclear fractions of HT22 cells exposed to oAβ showed ERK1/2 to have increased their nuclear localization in a process dependent on PI3K activity, since the PI3K inhibitor LY294002 diminished nuclear translocation of ERK1/2 (Fig. 4c).

Given that not only Akt but also ERK1/2 were found to translocate from the cytosol to the nucleus in the presence of oAβ, we also checked whether ERK1/2 were involved in Akt

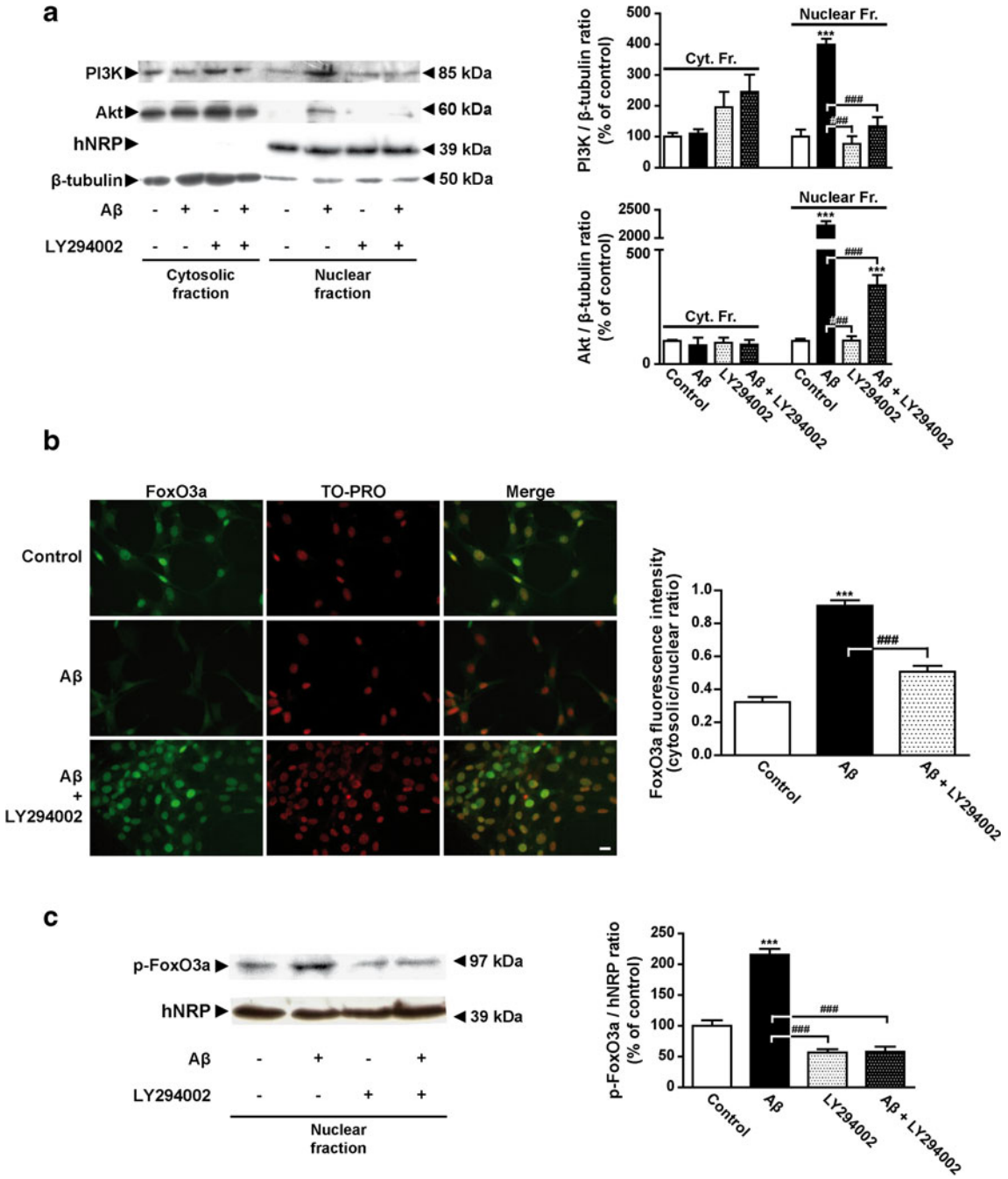

Fig. 3 PI3K/Akt/FoxO3a trafficking upon oAβ-exposure. HT22 neurons were incubated with 10 μM LY294002 or its vehicle for 30 min before exposure to oAβ and all along the 24-h treatment. **a** Subcellular fractions obtained from treated cells were analyzed by Western blot using antibodies against PI3K and Akt. hNRP was used as nuclear marker and β-tubulin was used as loading control. One representative blot of three different experiments is shown. Bands of proteins were quantified using scanning densitometry; the data in the *graphs on the right* represent the ratio between subcellular protein expression and β-tubulin, expressed as a percentage of the corresponding control condition. $^{***}p < 0.001$ for each condition with respect to the control, $^{###}p < 0.001$ shown in the picture; one-way ANOVA and Tukey's post hoc test. **b** After treatments, cells were processed for immunocytochemistry using antibody against FoxO3a. TO-PRO was used as nuclear marker. Pictures shown are representative of at least three different experiments. *Scale bar* 10 μm. Fluorescence of approximately 100–150 cells was quantified for each condition in each experiment. Fluorescence intensity quantification is shown on the *right*. $^{***}p < 0.001$ for each condition with respect to the control, $^{###}p < 0.001$ shown in the picture; one-way ANOVA and Tukey's post hoc test. **c** Nuclear fractions of treated cells were studied by Western blot. FoxO3a phosphorylation was assessed. hNRP was used as nuclear marker. Each blot is representative of at least three different experiments. Bands of proteins were quantified using scanning densitometry; the data in the *graph on the right* represent the ratio between phosphorylated FoxO3a and hNRP, expressed as a percentage of the corresponding control condition (mean ± SE of three different experiments). $^{***}p < 0.001$ for each condition with respect to the control, $^{###}p < 0.001$ shown in the picture; one-way ANOVA and Tukey's post hoc test

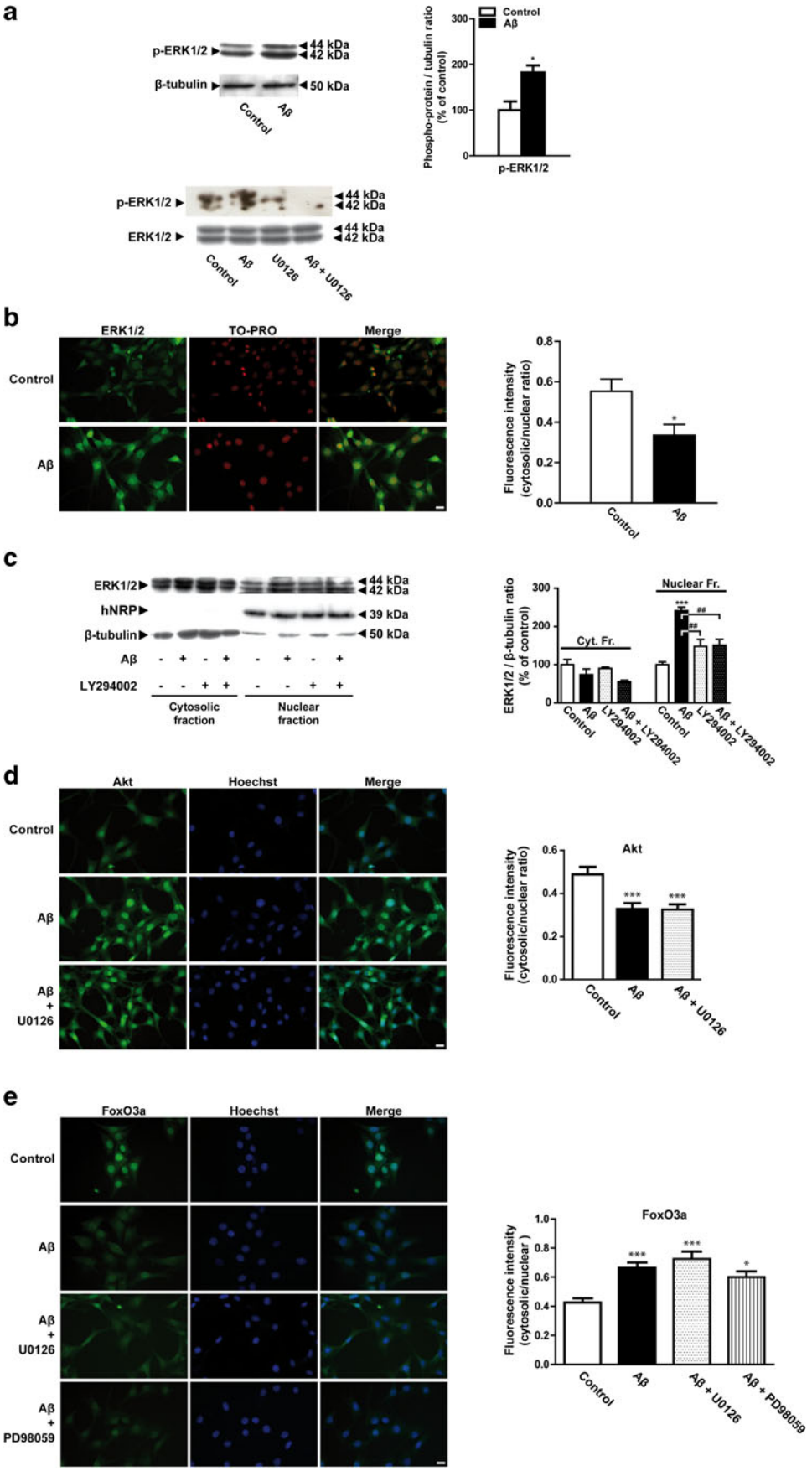
a
p-ERK1/2
β-tubulin
44 kDa
42 kDa
50 kDa
Control
Aβ
Phospho-protein / tubulin ratio (% of control)
p-ERK1/2
ERK1/2
U0126
Aβ + U0126
b
ERK1/2
TO-PRO
Merge
Fluorescence intensity (cytosolic/nuclear ratio)
c
hNRP
39 kDa
LY294002
Cytosolic fraction
Nuclear fraction
ERK1/2 / β-tubulin ratio (% of control)
Cyt. Fr.
Nuclear Fr.
d
Akt
Hoechst
Merge
e
FoxO3a
Aβ + PD98059

◀ **Fig. 4** Effects of oAβ exposure on ERK1/2 pathway. **a** Lysates from HT22 neurons exposed to oAβ or its vehicle were studied by Western blot. ERK1/2 phosphorylation and the effect of U0126 on ERK1/2 phosphorylation were evaluated. One representative blot of three different experiments is shown. Bands of proteins were quantified using scanning densitometry; the data in the *graph on the right* represent the ratio between phosphorylated ERK1/2 and β-tubulin, expressed as a percentage of the corresponding control condition (mean ± SE of three different experiments). $*p < 0.05$ with respect to the control; Student's *t* test. **b** Cells were grown onto coverslips, exposed to oAβ or its vehicle, and processed for immunocytochemistry using anti-ERK1/2 antibody. TO-PRO was used as nuclear marker. Pictures shown are representative of at least three different experiments. *Scale bars* 10 μm. Fluorescence of approximately 100–150 cells was quantified for each condition in each experiment. Fluorescence intensity quantification is shown on the *right*. $*p < 0.05$ with respect to the control; Student's *t* test. **c** Subcellular fractions of neurons incubated in the presence of 10 μM LY294002 (or its vehicle) and then exposed to oAβ or its vehicle were studied by Western blot using an antibody against ERK1/2. hNRP was used as nuclear marker and β-tubulin was used as loading control. Each blot is representative of at least three different experiments. Bands of proteins were quantified using scanning densitometry; the data in the *graph on the right* represent the ratio between ERK1/2 and β-tubulin in each subcellular fraction, expressed as a percentage of the corresponding control condition (mean ± SE of three different experiments). $***p < 0.001$ with respect to the control, $^{\#\#}p < 0.01$ shown in the picture; one-way ANOVA and Tukey's post hoc test. **d**, **e** HT22 cells were incubated with 10 μM U0126 or 10 μM PD98059 (or their vehicles) before the exposure to oAβ and all along the treatment. Immunocytochemistry analysis was performed using anti-Akt (**d**) and anti-FoxO3a (**e**) antibodies. TO-PRO was used as nuclear marker. The pictures shown are representative of three different experiments. *Scale bars* 10 μm. Fluorescence of approximately 100–150 cells was quantified for each condition in each experiment. Fluorescence intensity quantification is shown on the *right*. $*p < 0.05$, $***p < 0.001$ with respect to the control; one-way ANOVA and Tukey's post hoc test

and FoxO3a subcellular redistribution. For this purpose, we carried out the same experiment in the presence of U0126, a well-known inhibitor of MEK1/2. As shown in Fig. 4d, MEK1/2 inhibition (and thus the inhibition of ERK1/2) had no effect on oAβ-induced nuclear translocation of Akt. FoxO3a redistribution was also assessed in the presence of two different MEK inhibitors (U0126 and PD98059). The inhibition of ERK1/2 did not affect FoxO3a distribution pattern triggered by oAβ (Fig. 4e). These results demonstrate that oAβ-stimulated PI3K activity governs nuclear confinement of Akt and FoxO3a export from the nucleus and that these mechanisms are independent of ERK1/2 activation.

Consequences of oAβ Exposure on PI Signaling

Since PI3K, a PI kinase, seemed to play a major (ERK1/2-independent) role in the signaling against oligomeric Aβ, we next investigated the involvement of PI signaling in ERK1/2 activation. For this purpose, we used neomycin (an inhibitor of PI metabolism) and U73122 (a PI-PLC inhibitor) and then evaluated the ERK1/2 phosphorylation status in the presence of oAβ. Both experimental strategies demonstrated that oAβ-induced ERK1/2 activation was strictly dependent on PI metabolism (Fig. 5a, b). When investigating whether PI3K itself (as part of PI metabolism) was involved in oAβ-induced ERK1/2 activation, results showed that this lipid kinase does have a role in ERK1/2 activation since PI3K inhibition caused an even greater oAβ-induced phosphorylation (and activation) of ERK1/2 (Fig. 5c).

Role of PI Signaling in Neuronal Response to oAβ

Since our results clearly show that oAβ triggers neuronal PI signaling and that FoxO3a response is dependent on PI3K activity, we next sought to study whether PI-PLC activity exerts any effect on the nuclear exclusion of FoxO3a. For this purpose, we carried out the same experiment (with oAβ or its vehicle) both in the presence and absence of two inhibitors of PI-PLC, U73122 and edelfosine. Fluorescence microscopy studies show that the inhibition of PI-PLC promoted more oAβ-induced trafficking of FoxO3a out of the nucleus (Fig. 6a, b). For reinforcing the fact that PI-PLC pathway is activated by oAβ, the state of classical PKCs (α and β), well known downstream effectors of PI-PLC, was assessed. oAβ was able to trigger PKC priming process by phosphorylation, and the inhibition of PI-PLC with U73122 was able to revert this effect (Fig. 6c).

To further address the functional role of the aforementioned signaling pathways (PI3K/Akt, MEK1/2/ERK1/2, and PI-PLC) in hippocampal neuronal response to oAβ, cell viability assays (MTT reduction) and nucleic acid stain (SYTOX) with pharmacological manipulation of the signaling cascades were carried out. As observed in Fig. 7a, the inhibition of PI3K/Akt, MEK1/2/ERK1/2, and PI-PLC also caused an increase in cell death. Additionally, studies carried out with SYTOX probe (a cell death indicator) show that the inhibition of PI3K activity (LY294002) as well as PI metabolism (neomycin) caused an increase in the number of dead cells in the presence of Aβ (Fig. 7b).

Discussion

Historically, Aβ has been associated with cell toxicity and oxidative stress generation and for these reasons, has been attributed responsibility for AD onset and progression [31–33]. The mechanism proposed for Aβ-induced neurotoxicity includes the assembly of Aβ into oligomers and plaques [34]. In recent years, the possibility that Aβ oligomers, in addition to plaques, play an important role in AD progression [35] has gained weight. Although a great body of scientific literature reports Aβ accumulation in the AD brain causing neurodegeneration [36], no strong clinical correlation between plaque deposition and cognitive impairment during AD has been demonstrated [37]. Moreover, a negative correlation

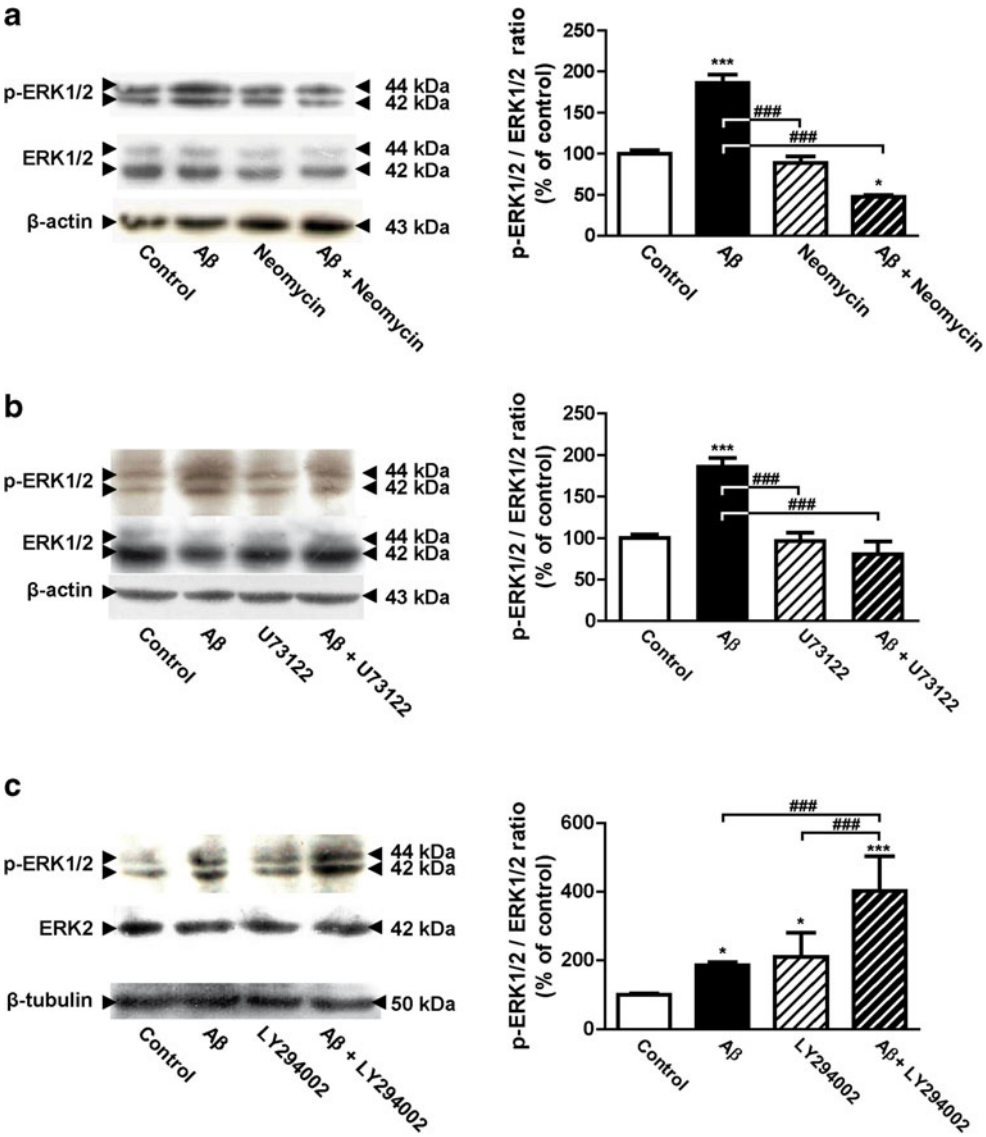

Fig. 5 Involvement of PI metabolism on oAβ-triggered ERK1/2 activation. HT22 neurons were incubated in the presence of 200 μM neomycin (**a**), 10 μM U73122 (**b**), and 10 μM LY294002 (**c**) or their vehicles for 30 min before the exposure to oAβ and all along the 24-h treatment. Lysates were studied by Western blot using antibodies against phospho-ERK1/2 and ERK1/2. β-actin and β-tubulin were used as loading control. One representative blot of three different experiments is shown. Bands of proteins were quantified using scanning densitometry; the data in the *graphs on the right* represent the ratio between phospho-ERK1/2 and ERK1/2, expressed as a percentage of the corresponding control condition (mean ± SE of three different experiments). $^{*}p < 0.05$, $^{***}p < 0.001$ for each condition with respect to the control; $^{\#\#\#}p < 0.001$ shown in the picture; one-way ANOVA and Tukey's post hoc test

between Aβ deposition and cerebral oxidative injury has been shown by Nunomura et al. [38]. On the basis of these findings, Aβ deposition has been proposed to be a protective response rather than the cause of the disease [39, 40], and the original model is now under debate [33].

We have previously characterized the effects of oAβ both alone and combined with iron and/or copper on synaptic viability and signaling [15]. In particular, we demonstrated that synaptic PI3K/Akt and ERK1/2 pathways are activated in response to oAβ-induced injury. In the present study, we characterized the effect of oAβ on hippocampal neurons, in order to understand the unanswered questions surrounding oAβ-triggered PI3K/Akt and ERK1/2 signaling. Exogenous oAβ (nanomolar range) did not cause any noticeable damage to HT22 hippocampal neurons compared to the control condition; no morphological alterations (neither subtle nor gross), no decrease in neuronal viability, no increase in lipid peroxidation, cellular oxidants or caspase 3 activity, and no membrane damage (neither disruption of plasma membrane integrity nor alteration of the lipid order of the membrane) were observed. In agreement with our results, it has been shown that exogenous Aβ induces cell death only in the micromolar range [9, 41–43]. Moreover, Aβ infusion in organotypic hippocampal slice cultures showed no clear signs of cell death [44].

Interestingly, oAβ behavior in our study was similar to that reported for neurotrophic factors (many of whose main target is the PI3K/Akt pathway) in neurons. Of note, oAβ has been shown to bind to different cell surface receptors and compete with their ligands (for example, BDNF), all of which results in brain dysfunction associated with AD [43]. For instance, oAβ has been demonstrated to bind to β2 adrenergic receptor, affecting glutamatergic regulation of synaptic activities via PKA signaling [8, 45, 46]. In addition, murine PirB (paired immunoglobulin-like receptor B) and its human ortholog LilrB2 (leukocyte immunoglobulin-like receptor B2)

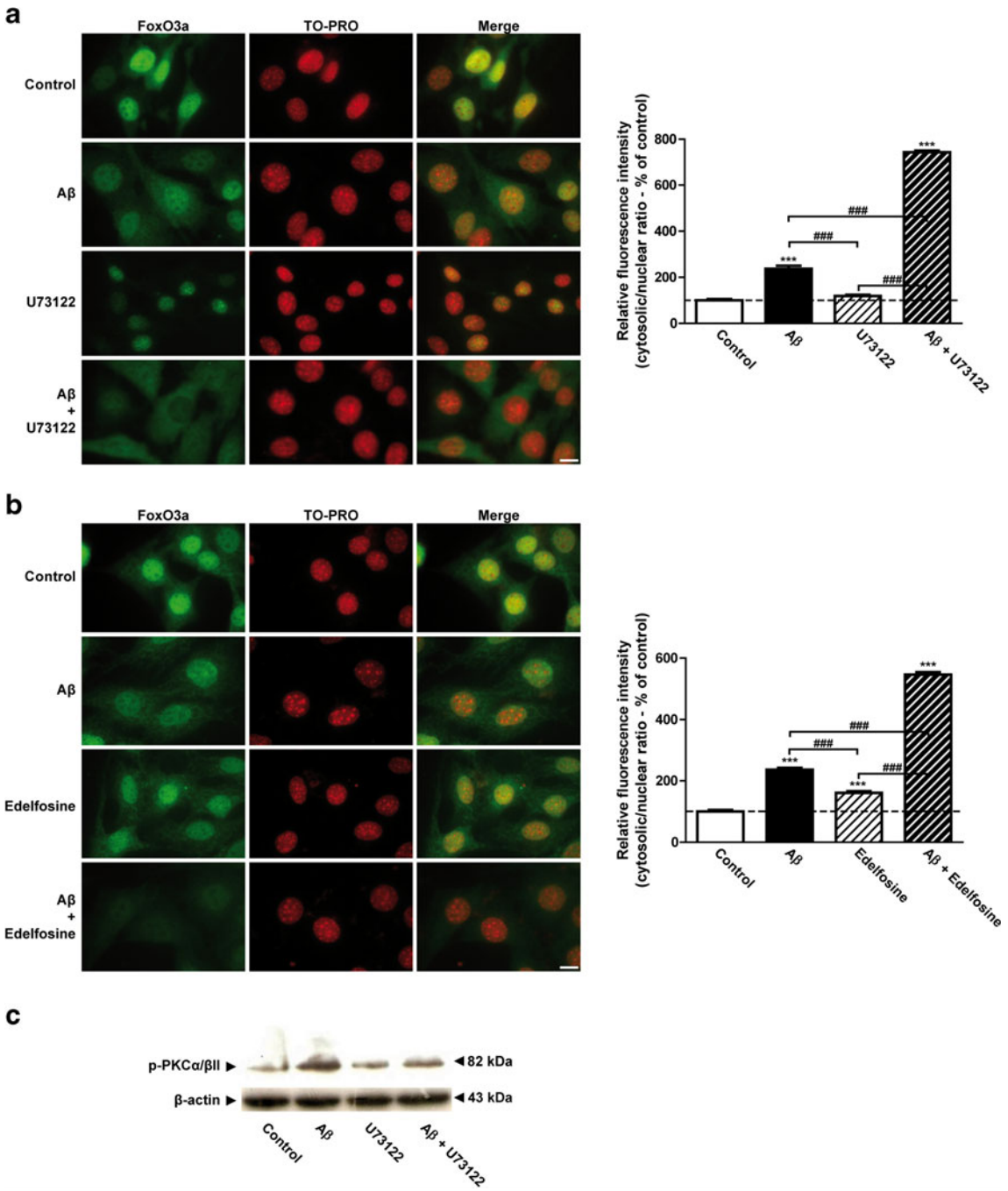

Fig. 6 Role of PI-PLC in oAβ-induced FoxO3a trafficking. **a** Cells were grown onto coverslips, incubated in the presence of 10 μM U73122 or its vehicle for 30 min before the exposure to oAβ or its vehicle, and processed for immunocytochemistry using anti-FoxO3a antibody. TO-PRO was used as a nuclear marker. Pictures shown are representative of at least three different experiments. *Scale bars* 10 μm. Fluorescence of approximately 100–150 cells was quantified for each condition in each experiment. The *graph on the right* represents the ratio between cytosolic and nuclear fluorescence intensity, expressed as a percentage of the corresponding control condition (mean ± SE of three different experiments). $^{***}p < 0.001$ for each condition with respect to the control; $^{\#\#\#}p < 0.001$ shown in the picture; one-way ANOVA and Tukey's post hoc test. **b** Similar experiments were performed using another PI-PLC inhibitor (edelfosine, 2.5 μM). **c** Western blots of cellular lysates were used for testing PKC α/βII phosphorylation

have been demonstrated to bind Aβ oligomers with affinity in the nanomolar range [47], and the cellular prion protein (PrP^C) has been demonstrated to be an oAβ receptor (in a mechanism coupled to mGluR5), with nanomolar affinity for Aβ oligomers [48–51]. Moreover, oAβ has also been shown to bind to the nicotinic acetylcholine receptor [52–56].

Based on this body of evidence showing direct binding of oAβ to cell surface receptors, and taking into account that (i) PI3K is known to be activated, among other stimuli, by

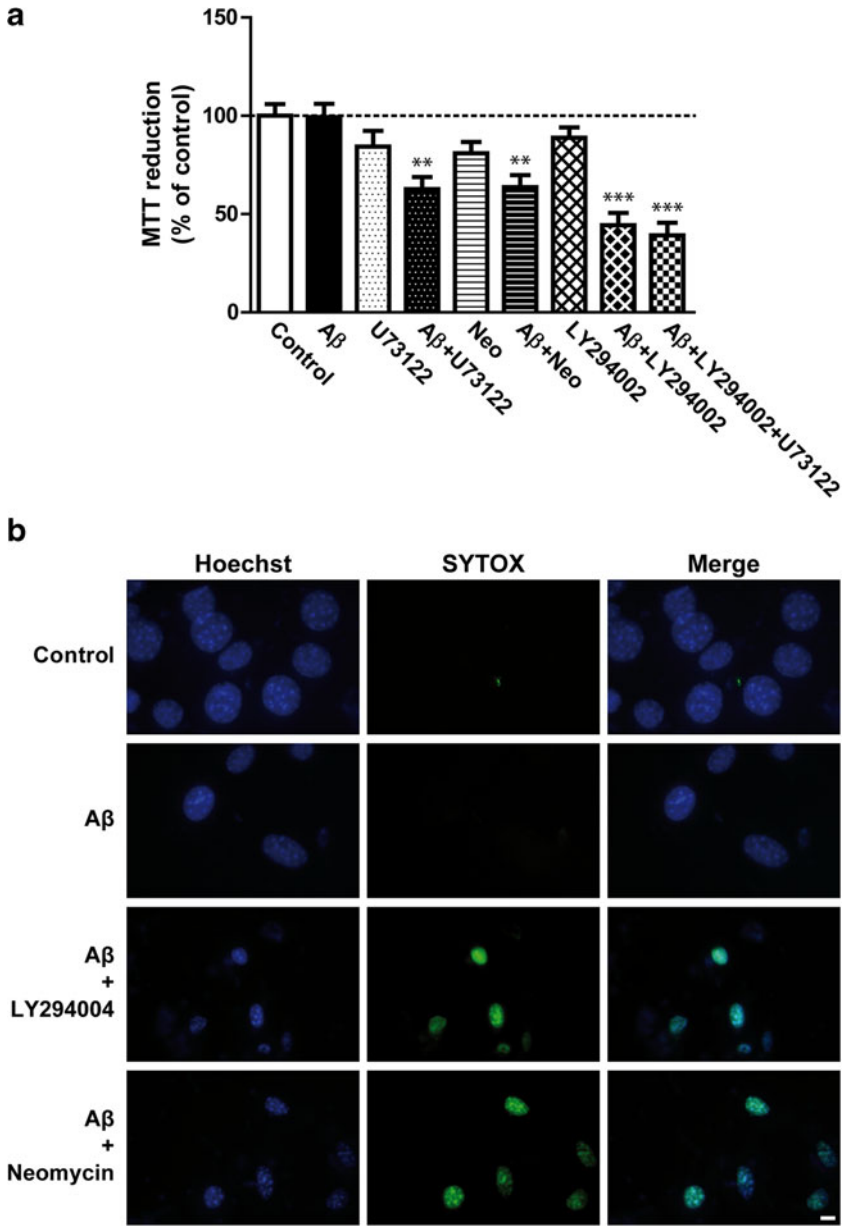

Fig. 7 Functional role of phosphoinositides in cellular response to oAβ. **a** MTT reduction assay. HT22 cells were treated with different inhibitors (U73122, neomycin -Neo-, and LY294002) or their vehicles for 30 min and then exposed to oAβ (or its vehicle), and cell viability was assessed as specified in "Materials and Methods" section. Results are expressed as a percentage of the control and represent mean ± SE ($n = 3–5$). $^{**}p < 0.01$, $^{***}p < 0.001$ for each condition with respect to the control; one-way ANOVA and Tukey's post hoc test. **b** SYTOX *green* staining of neurons. Cells were grown onto coverslips, incubated with 200 μM neomycin or 10 μM LY294002 for 30 min, and then treated with oAβ or its vehicle. Nuclei were double stained. Hoechst was used as nuclear marker and SYTOX as a marker of death cells. Pictures shown are representative of three different experiments

insulin; (ii) ERK1/2 has been reported to be involved in oAβ-induced impairment of insulin signaling [57]; (iii) Aβ and insulin are both amyloidogenic peptides with common domains recognized by insulin receptor and insulin degrading enzyme [58, 59]; and (iv) an impairment of glucose metabolism has been found during the progression of AD [60], we proceeded to investigate insulin receptor as a responsive pathway to oAβ. In our assays, oAβ triggered the phosphorylation (which represents the activation) of insulin receptor to the same extent as it triggered the phosphorylation of Akt. In contrast with our results, several reports have described an impairment of insulin signaling in different biological models exposed to Aβ [57, 59, 61]. A variety of factors could explain the discrepancies with the results presented here, such as the concentration and aggregation state of Aβ, the cellular model used, and the time of exposure. Interestingly, and in agreement with our results, Zhao et al. [61] show an increase in Aβ-induced phosphorylation of insulin receptor in the absence of the hormone. Our results on the activation of insulin receptor are a further addition to the evidence showing that oAβ triggers intracellular signaling by receptor-mediated mechanisms.

We have previously found that mild neuronal damage induced by oxidative stress is accompanied by the activation and subcellular redistribution of PI3K/Akt pathway and FoxO3a transcription factor, thus triggering a neuroprotective mechanism [16]. Indeed, we found oAβ-induced FoxO3a trafficking to be dependent on PI3K activity. Thus, the PI3K-dependent inactivation of FoxO3a found in the presence of oAβ may represent a neuroprotective mechanism operating

prior to the appearance of any clear sign of threat. In this connection, other reports have attributed a protective role to PI3K-mediated FoxO3a inactivation and subcellular redistribution [16, 62–64].

oAβ also triggered ERK1/2 activation, which was found to be dependent on PI-PLC activity or, in a broader sense, on PI availability, since the inhibition of either PI-PLC or PI metabolism abolished oAβ-triggered ERK1/2 activation, whereas PI3K inhibition potentiated it. Moreover, phosphorylation of PKCα/βII was also found to increase in the presence of oAβ (Fig. 6c). Since diacylglycerol (DAG) has been shown to activate ERK1/2 (usually by either PKC-mediated and/or RasGRP/Ras/Raf-mediated mechanisms), our results are congruent with ERK1/2 being activated by an oAβ-triggered DAG-generating PI-PLC-dependent mechanism. Together, these data clearly demonstrate a major role for phosphoinositide-dependent signaling in neuronal response to oAβ.

However, the relationship between phosphoinositides, nuclear exclusion of FoxO3a, and cell survival remains unclear. FoxO3a trafficking out of the nuclear compartment is known to be an Akt-dependent event associated with cell survival [16, 62], so it is logical to assume that the higher the level of Akt activity, the more FoxO3a is trafficked from the nucleus as a pro-life signal. On the other hand, our studies also showed PI-PLC to be a protective pathway; however, less nuclear and more cytosolic FoxO3a content was observed when PI-PLC was inhibited in oAβ-challenged neurons compared to neurons only treated with oAβ. Intriguingly, PI-PLC inhibition decreased neuronal survival. Our results shed light on neuronal survival signaling in response to oAβ, demonstrating that a strict balance between PI3K and PI-PLC intracellular targets is necessary. In the light of our results, we propose phosphatidylinositol bis-phosphate (PIP_2) as the key mediator of neuronal response to oAβ; inhibition of PI3K makes more substrate available for PI-PLC activity and the consequent activation of ERK1/2, whereas on the contrary, inhibition of PI-PLC makes more substrate available for PI3K activity, Akt activation, and the concomitant trafficking of FoxO3a out of the nucleus (Fig. 8).

ERK1/2 has been shown to regulate both FoxO3a nuclear exclusion and ubiquitin-proteasome mediated degradation of FoxO3a through different mechanisms of phosphorylation [65]. However, oAβ-induced PI-PLC-dependent ERK1/2 activation is not related to FoxO3a nuclear exclusion in our study, suggesting that the activation and cellular redistribution of ERK1/2 participate in neuronal protective mechanisms that are not directly related to FoxO3a trafficking. However, it cannot be ruled out that the oAβ-induced increase in cytosolic FoxO3a content upon PI-PLC inhibition is indeed due to the inhibition of ERK1/2-dependent FoxO3a degradation.

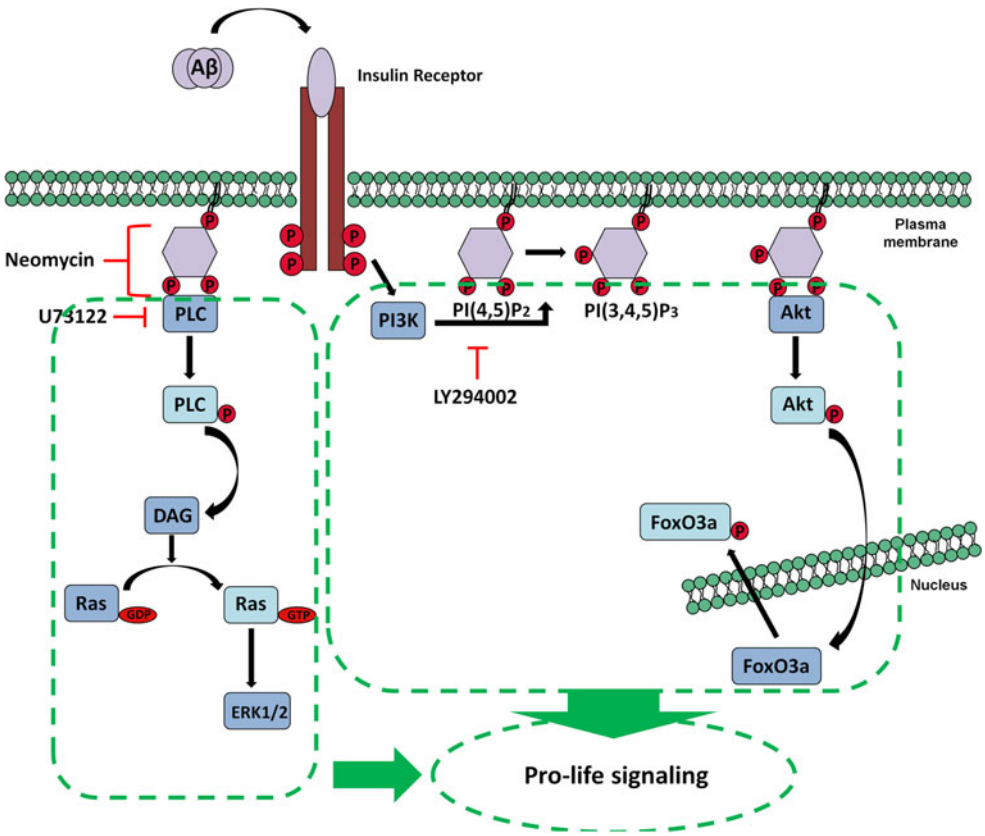

Fig. 8 Graph depicting the PI-dependent signaling pathways triggered in the neuronal response to oAβ

Our results are the first evidence of a key role for phosphoinositides in neuronal response to oAβ. It comes to light that PIP_2 is a convergence point of signaling pathways (PI3K/Akt and PI-PLC/ERK1/2) crucial for determining cellular fate and whose redundant triggering guarantees protective mechanisms to react against oAβ in the nanomolar range. Our work is the starting point for a new hypothesis in the study of neuronal effects of oAβ; could Aβ be a very early neuroprotective moiety appearing ahead of ultimate AD collapse?

Acknowledgments We thank Dr. Charles Glabe (Department of Molecular Biology and Biochemistry, University of California, Irvine, USA) for kindly providing OC and A11 antibodies. This work was supported by Universidad Nacional del Sur (PGI 24/B179), Agencia Nacional de Promoción Científica y Tecnológica (ANPCyT; PICT-2010-0936 and PICT-2013-0987), and Consejo Nacional de Investigaciones Científicas y Técnicas (CONICET; PIP 11220120100251).

References

1. Klein WL (2013) Synaptotoxic amyloid-beta oligomers: a molecular basis for the cause, diagnosis, and treatment of Alzheimer's disease? J Alzheimers Dis 33(Suppl 1):S49–S65
2. Hartley DM, Walsh DM, Ye CP, Diehl T, Vasquez S, Vassilev PM, Teplow DB, Selkoe DJ (1999) Protofibrillar intermediates of amyloid beta-protein induce acute electrophysiological changes and progressive neurotoxicity in cortical neurons. J Neurosci 19:8876–8884
3. Kamenetz F, Tomita T, Hsieh H, Seabrook G, Borchelt D, Iwatsubo T, Sisodia S, Malinow R (2003) APP processing and synaptic function. Neuron 37:925–937
4. Nimmrich V, Grimm C, Draguhn A, Barghorn S, Lehmann A, Schoemaker H, Hillen H, Gross G et al (2008) Amyloid beta oligomers (A beta(1–42) globulomer) suppress spontaneous synaptic activity by inhibition of P/Q-type calcium currents. J Neurosci 28:788–797
5. Shankar GM, Li S, Mehta TH, Garcia-Munoz A, Shepardson NE, Smith I, Brett FM, Farrell MA et al (2008) Amyloid-beta protein dimers isolated directly from Alzheimer's brains impair synaptic plasticity and memory. Nat Med 14:837–842
6. Ye C, Walsh DM, Selkoe DJ, Hartley DM (2004) Amyloid beta-protein induced electrophysiological changes are dependent on aggregation state: N-methyl-D-aspartate (NMDA) versus non-NMDA receptor/channel activation. Neurosci Lett 366:320–325
7. Xia M, Cheng X, Yi R, Gao D, Xiong J (2014) The binding receptors of Abeta: an alternative therapeutic target for Alzheimer's disease. Mol Neurobiol 1–17
8. Wang D, Yuen EY, Zhou Y, Yan Z, Xiang YK (2011) Amyloid beta peptide-(1–42) induces internalization and degradation of beta2 adrenergic receptors in prefrontal cortical neurons. J Biol Chem 286: 31852–31863
9. Jin Y, Tsuchiya A, Kanno T, Nishizaki T (2015) Amyloid-beta peptide increases cell surface localization of alpha7 ACh receptor to protect neurons from amyloid beta-induced damage. Biochem Biophys Res Commun 468:157–160
10. Inestrosa NC, Godoy JA, Vargas JY, Arrazola MS, Rios JA, Carvajal FJ, Serrano FG, Farias GG (2013) Nicotine prevents synaptic impairment induced by amyloid-beta oligomers through alpha7-nicotinic acetylcholine receptor activation. Neuromolecular Med 15:549–569
11. Sola VF, Kedikian G, Heredia L, Heredia F, Anel AD, Rosa AL, Lorenzo A (2009) Amyloid-beta precursor protein mediates neuronal toxicity of amyloid beta through Go protein activation. Neurobiol Aging 30:1379–1392
12. Cecon E, Chen M, Marcola M, Fernandes PA, Jockers R, Markus RP (2015) Amyloid beta peptide directly impairs pineal gland melatonin synthesis and melatonin receptor signaling through the ERK pathway. FASEB J 29:2566–2582
13. Bignante EA, Heredia F, Morfini G, Lorenzo A (2013) Amyloid beta precursor protein as a molecular target for amyloid beta—induced neuronal degeneration in Alzheimer's disease. Neurobiol Aging 34:2525–2537
14. Valles AS, Borroni MV, Barrantes FJ (2014) Targeting brain alpha7 nicotinic acetylcholine receptors in Alzheimer's disease: rationale and current status. CNS Drugs 28:975–987
15. Uranga RM, Giusto NM, Salvador GA (2010) Effect of transition metals in synaptic damage induced by amyloid beta peptide. Neuroscience 170:381–389
16. Uranga RM, Katz S, Salvador GA (2013) Enhanced phosphatidylinositol 3-kinase (PI3K)/Akt signaling has pleiotropic targets in hippocampal neurons exposed to iron-induced oxidative stress. J Biol Chem 288:19773–19784
17. O'Neill C, Kiely AP, Coakley MF, Manning S, Long-Smith CM (2012) Insulin and IGF-1 signalling: longevity, protein homoeostasis and Alzheimer's disease. Biochem Soc Trans 40: 721–727
18. Parodi J, Sepulveda FJ, Roa J, Opazo C, Inestrosa NC, Aguayo LG (2010) Beta-amyloid causes depletion of synaptic vesicles leading to neurotransmission failure. J Biol Chem 285:2506–2514
19. Sepulveda FJ, Opazo C, Aguayo LG (2009) Alzheimer beta-amyloid blocks epileptiform activity in hippocampal neurons. Mol Cell Neurosci 41:420–428
20. Kayed R, Head E, Sarsoza F, Saing T, Cotman CW, Necula M, Margol L, Wu J et al (2007) Fibril specific, conformation dependent antibodies recognize a generic epitope common to amyloid fibrils and fibrillar oligomers that is absent in prefibrillar oligomers. Mol Neurodegener 2:18
21. Uranga RM, Mateos MV, Giusto NM, Salvador GA (2007) Activation of phosphoinositide-3 kinase/Akt pathway by FeSO4 in rat cerebral cortex synaptic endings. J Neurosci Res 85:2924–2932
22. Uranga RM, Giusto NM, Salvador GA (2009) Iron-induced oxidative injury differentially regulates PI3K/Akt/GSK3beta pathway in synaptic endings from adult and aged rats. Toxicol Sci 111:331–344
23. Hanzel CE, Verstraeten SV (2009) Tl(I) and Tl(III) activate both mitochondrial and extrinsic pathways of apoptosis in rat pheochromocytoma (PC12) cells. Toxicol Appl Pharmacol 236:59–70
24. Bradford MM (1976) A rapid and sensitive method for the quantitation of microgram quantities of protein utilizing the principle of protein-dye binding. Anal Biochem 72:248–254
25. Parasassi T, De SG, d'Ubaldo A, Gratton E (1990) Phase fluctuation in phospholipid membranes revealed by Laurdan fluorescence. Biophys J 57:1179–1186
26. Parasassi T, De SG, Ravagnan G, Rusch RM, Gratton E (1991) Quantitation of lipid phases in phospholipid vesicles by the generalized polarization of Laurdan fluorescence. Biophys J 60:179–189
27. Shinitzky MYY (1982) Lipid fluidity at the submacroscopic level: determination by fluorescence polarization. Chem Phys Lipids 30: 261–282
28. Dignam JD, Lebovitz RM, Roeder RG (1983) Accurate transcription initiation by RNA polymerase II in a soluble extract from isolated mammalian nuclei. Nucleic Acids Res 11:1475–1489
29. Osborn L, Kunkel S, Nabel GJ (1989) Tumor necrosis factor alpha and interleukin 1 stimulate the human immunodeficiency virus enhancer by activation of the nuclear factor kappa B. Proc Natl Acad Sci U S A 86:2336–2340

30. Kaiser RD, London E (1998) Location of diphenylhexatriene (DPH) and its derivatives within membranes: comparison of different fluorescence quenching analyses of membrane depth. Biochemistry 37:8180–8190
31. Kadowaki H, Nishitoh H, Urano F, Sadamitsu C, Matsuzawa A, Takeda K, Masutani H, Yodoi J et al (2005) Amyloid beta induces neuronal cell death through ROS-mediated ASK1 activation. Cell Death Differ 12:19–24
32. Lambert JC, Amouyel P (2011) Genetics of Alzheimer's disease: new evidences for an old hypothesis? Curr Opin Genet Dev 21: 295–301
33. Mondragon-Rodriguez S, Perry G, Zhu X, Boehm J (2012) Amyloid beta and tau proteins as therapeutic targets for Alzheimer's disease treatment: rethinking the current strategy. Int J Alzheimers Dis 2012:630182
34. Pike CJ, Burdick D, Walencewicz AJ, Glabe CG, Cotman CW (1993) Neurodegeneration induced by beta-amyloid peptides in vitro: the role of peptide assembly state. J Neurosci 13:1676–1687
35. Miñano-Molina AJ, Espana J, Martin E, Barneda-Zahonero B, Fado R, Sole M, Trullas R, Saura CA et al (2011) Soluble oligomers of amyloid-beta peptide disrupt membrane trafficking of alpha-amino-3-hydroxy-5-methylisoxazole-4-propionic acid receptor contributing to early synapse dysfunction. J Biol Chem 286:27311–27321
36. Jucker M, Walker LC (2011) Pathogenic protein seeding in Alzheimer disease and other neurodegenerative disorders. Ann Neurol 70:532–540
37. Arriagada PV, Growdon JH, Hedley-Whyte ET, Hyman BT (1992) Neurofibrillary tangles but not senile plaques parallel duration and severity of Alzheimer's disease. Neurology 42:631–639
38. Nunomura A, Tamaoki T, Tanaka K, Motohashi N, Nakamura M, Hayashi T, Yamaguchi H, Shimohama S et al (2010) Intraneuronal amyloid beta accumulation and oxidative damage to nucleic acids in Alzheimer disease. Neurobiol Dis 37:731–737
39. Castellani RJ, Lee HG, Siedlak SL, Nunomura A, Hayashi T, Nakamura M, Zhu X, Perry G et al (2009) Reexamining Alzheimer's disease: evidence for a protective role for amyloid-beta protein precursor and amyloid-beta. J Alzheimers Dis 18: 447–452
40. Obrenovich ME, Joseph JA, Atwood CS, Perry G, Smith MA (2002) Amyloid-beta: a (life) preserver for the brain. Neurobiol Aging 23:1097–1099
41. Gargantini E, Lazzari L, Settanni F, Taliano M, Trovato L, Gesmundo I, Ghigo E, Granata R (2015) Obestatin promotes proliferation and survival of adult hippocampal progenitors and reduces amyloid-beta-induced toxicity. Mol Cell Endocrinol
42. Lilja AM, Porras O, Storelli E, Nordberg A, Marutle A (2011) Functional interactions of fibrillar and oligomeric amyloid-beta with alpha7 nicotinic receptors in Alzheimer's disease. J Alzheimers Dis 23:335–347
43. Tong L, Balazs R, Thornton PL, Cotman CW (2004) Beta-amyloid peptide at sublethal concentrations downregulates brain-derived neurotrophic factor functions in cultured cortical neurons. J Neurosci 24:6799–6809
44. Bahr BA, Hoffman KB, Yang AJ, Hess US, Glabe CG, Lynch G (1998) Amyloid beta protein is internalized selectively by hippocampal field CA1 and causes neurons to accumulate amyloidogenic carboxyterminal fragments of the amyloid precursor protein. J Comp Neurol 397:139–147
45. Wang D, Govindaiah G, Liu R, De Arcangelis V, Cox CL, Xiang YK (2010) Binding of amyloid beta peptide to beta2 adrenergic receptor induces PKA-dependent AMPA receptor hyperactivity. FASEB J 24:3511–3521
46. Wang D, Fu Q, Zhou Y, Xu B, Shi Q, Igwe B, Matt L, Hell JW et al (2013) Beta2 adrenergic receptor, protein kinase A (PKA) and c-Jun N-terminal kinase (JNK) signaling pathways mediate tau pathology in Alzheimer disease models. J Biol Chem 288:10298–10307
47. Kim T, Vidal GS, Djurisic M, William CM, Birnbaum ME, Garcia KC, Hyman BT, Shatz CJ (2013) Human LilrB2 is a beta-amyloid receptor and its murine homolog PirB regulates synaptic plasticity in an Alzheimer's model. Science 341:1399–1404
48. Lauren J, Gimbel DA, Nygaard HB, Gilbert JW, Strittmatter SM (2009) Cellular prion protein mediates impairment of synaptic plasticity by amyloid-beta oligomers. Nature 457:1128–1132
49. Lauren J (2014) Cellular prion protein as a therapeutic target in Alzheimer's disease. J Alzheimers Dis 38:227–244
50. Renner M, Lacor PN, Velasco PT, Xu J, Contractor A, Klein WL, Triller A (2010) Deleterious effects of amyloid beta oligomers acting as an extracellular scaffold for mGluR5. Neuron 66:739–754
51. Um JW, Kaufman AC, Kostylev M, Heiss JK, Stagi M, Takahashi H, Kerrisk ME, Vortmeyer A et al (2013) Metabotropic glutamate receptor 5 is a coreceptor for Alzheimer abeta oligomer bound to cellular prion protein. Neuron 79:887–902
52. Fu W, Jhamandas JH (2003) Beta-amyloid peptide activates non-alpha7 nicotinic acetylcholine receptors in rat basal forebrain neurons. J Neurophysiol 90:3130–3136
53. Liu Q, Kawai H, Berg DK (2001) Beta-amyloid peptide blocks the response of alpha 7-containing nicotinic receptors on hippocampal neurons. Proc Natl Acad Sci U S A 98:4734–4739
54. Liu Q, Huang Y, Xue F, Simard A, DeChon J, Li G, Zhang J, Lucero L et al (2009) A novel nicotinic acetylcholine receptor subtype in basal forebrain cholinergic neurons with high sensitivity to amyloid peptides. J Neurosci 29:918–929
55. Pettit DL, Shao Z, Yakel JL (2001) Beta-amyloid(1–42) peptide directly modulates nicotinic receptors in the rat hippocampal slice. J Neurosci 21:RC120
56. Dineley KT, Bell KA, Bui D, Sweatt JD (2002) Beta-amyloid peptide activates alpha 7 nicotinic acetylcholine receptors expressed in *Xenopus oocytes*. J Biol Chem 277:25056–25061
57. Zhang Q, Guo S, Zhang X, Tang S, Wang L, Han X, Shao W, Cong L et al (2015) Amyloid beta oligomer-induced ERK1/2-dependent serine 636/639 phosphorylation of insulin receptor substrate-1 impairs insulin signaling and glycogen storage in human astrocytes. Gene 561:76–81
58. Kurochkin IV, Goto S (1994) Alzheimer's beta-amyloid peptide specifically interacts with and is degraded by insulin degrading enzyme. FEBS Lett 345:33–37
59. Xie L, Helmerhorst E, Taddei K, Plewright B, Van BW, Martins R (2002) Alzheimer's beta-amyloid peptides compete for insulin binding to the insulin receptor. J Neurosci 22:RC221
60. Minoshima S, Cross DJ, Foster NL, Henry TR, Kuhl DE (1999) Discordance between traditional pathologic and energy metabolic changes in very early Alzheimer's disease. Pathophysiological implications. Ann N Y Acad Sci 893:350–352
61. Zhao WQ, De Felice FG, Fernandez S, Chen H, Lambert MP, Quon MJ, Krafft GA, Klein WL (2008) Amyloid beta oligomers induce impairment of neuronal insulin receptors. FASEB J 22:246–260
62. Brunet A, Bonni A, Zigmond MJ, Lin MZ, Juo P, Hu LS, Anderson MJ, Arden KC et al (1999) Akt promotes cell survival by phosphorylating and inhibiting a Forkhead transcription factor. Cell 96:857–868
63. Fukunaga K, Ishigami T, Kawano T (2005) Transcriptional regulation of neuronal genes and its effect on neural functions: expression and function of Forkhead transcription factors in neurons. J Pharmacol Sci 98:205–211
64. Nakae J, Park BC, Accili D (1999) Insulin stimulates phosphorylation of the Forkhead transcription factor FKHR on serine 253 through a wortmannin-sensitive pathway. J Biol Chem 274: 15982–15985
65. Yang JY, Zong CS, Xia W, Yamaguchi H, Ding Q, Xie X, Lang JY, Lai CC et al (2008) ERK promotes tumorigenesis by inhibiting FOXO3a via MDM2-mediated degradation. Nat Cell Biol 10: 138–148